AAS 20-579

AN ENERGY-INFORMED ADAPTIVE ALGORITHM FOR LOW-THRUST SPACECRAFT CISLUNAR TRAJECTORY DESIGN

Bonnie Prado Pino* **and Kathleen C. Howell†**

A near-term goal for the expansion of activities in the Earth-Moon neighborhood is the capability to maintain a facility near the Moon that serves as a staging node for excursions to other cislunar destinations. Support for low-thrust vehicles in this dynamically sensitive region include functional requirements that depend upon the scientific mission constraints and on the limitations introduced by the physical capabilities of the spacecraft[1]. This investigation offers an adaptive strategy for generating locally optimal solutions for low-thrust spacecraft in the lunar vicinity, by exploiting the energy parametrization of multi-body families of orbits. Results are validated in a higher-fidelity ephemeris model and are demonstrated for a variety of transfers with a wide range of thrust acceleration levels. The methodology proves successful for achieving large orbital plane changes evolving entirely within the lunar vicinity, as well as for generating suitable initial guesses for long spiral transfers approaching low lunar orbits.

INTRODUCTION

Within the past decade and with the development of the most recent propulsion technologies, the size of payloads —or secondary vehicles— are being reduced to smaller spacecraft that require very limited thrust force magnitudes for maintenance in a specific orbit and/or for its attitude to be controlled, e.g., CubeSats[2,3]. The time required for such vehicles to perform maneuvers and, when necessary, escape the gravitational attraction of the primary bodies, is considerably longer as compared to vehicles propelled by chemical engines[4,5]. The thrust acceleration levels then become a decisive factor in trajectory design for vehicles propelled by low-thrust engines in cislunar space. But, beyond the capabilities to deliver and maintain a low-thrust spacecraft in a particular orbit, support for the main mission requirements might also necessitate the capability to transfer to other cislunar destinations for various tasks.

Within the context of trajectory design for vehicles powered by low-thrust engines in the vicinity of the Moon, the generation of locally optimal solutions for the control history of the thrust orientation vector is a non-trivial process, challenging in terms of both time-of-flight and propellant usage[6,7]. Multiple geometries exist in the design of low-cost low-thrust transfers between libration point orbits[5]. These geometries depend upon the physical constraints of the low-thrust engine, in terms of magnitude and orientation of the thrust vector, and on the stability characteristics of the destination and departure orbits. Within the context of the unperturbed Circular Restricted Three Body Problem (CRTBP), a model where the primary bodies are assumed to be point masses, the

*PhD Candidate, Astrodynamics and Space Applications, School of Aeronautics and Astronautics, College of Engineering, Purdue University, West Lafayette, IN 47906. bpradopi@purdue.edu

†Hsu Lo Distinguished Professor, School of Aeronautics and Astronautics, College of Engineering, Purdue University, West Lafayette, IN 47906. howell@purdue.edu

dynamical equations of motion that describe the behavior of a spacecraft in this system are time-invariant[8,9]. With the introduction of a thrust force, the time dependency also induces an energy variation. In this investigation, the geometries of the transfer trajectories for a low-thrust vehicle, are described in terms of three types of categories and illustrated in Figure 1:

- Direct transfers: transfers that resemble the geometry of minimum impulsive burn trajectories
- Interior Transfers or Sliding-Type Geometry: transfers that access multiple members of periodic orbit families, to generate solutions that do not depart the vicinity of interest
- Exterior Transfers or Escape-Type Geometry: trajectories that utilize exterior manifold arcs and/or exterior-type orbits, to generate transfers that depart the vicinity of interest with a possible return

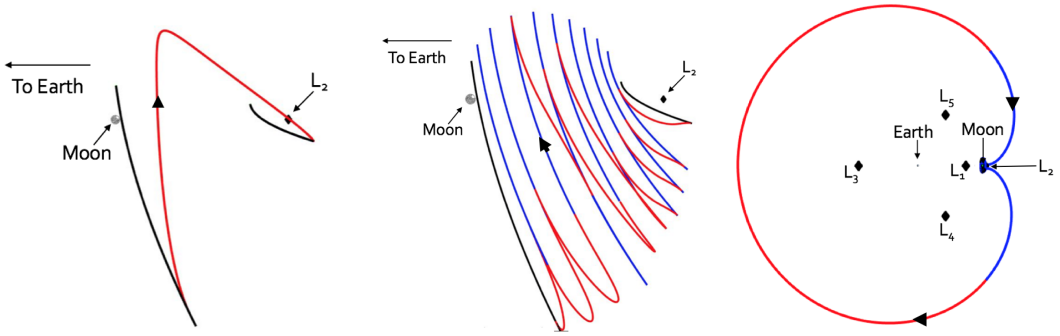

(a) Direct transfers

(b) Interior Transfers or Sliding-Type Geometry

(c) Exterior Transfers or Escape-Type Geometry

Figure 1. An illustration of the different types of geometries for low-thrust transfers between libration point orbits (red reflects active thrusters; blue arcs are coasting)

The sliding algorithm described in this investigation accommodates all three categories of transfer geometries by exploiting an orbit chaining framework[4].

This investigation focuses on the development of an adaptive sliding algorithm as the fundamental approach to generate trajectories. Transfers with a sliding-type geometry exploit natural arcs within an orbit chaining framework and offer the capability to identify interior transfer geometries when manifolds arcs are not available. The orbit chaining framework then allows any periodic orbit that exists within the model to be leveraged as an intermediate arc to generate suitable initial guesses for all the various type of transfers: (i) to generate direct transfers, the adaptive sliding algorithm selects the values for the maximum thrust acceleration level, and the engine specific impulse, to resemble those of chemical engines; (ii) to compute interior transfers, the adaptive sliding algorithm utilizes arcs from families of periodic orbits within the vicinity of interest; (iii) to produce exterior transfers, the adaptive sliding algorithm exploits arcs from families of periodic orbits that experience long transits throughout the Earth-Moon system.

The complexity in designing these transfer trajectories is first addressed by exploring the dynamics for the low-thrust spacecraft in an environment where the motion of the vehicle is described in a multi-body scenario. The adaptive sliding algorithm is formulated within this context. Thus, the various energy levels and stability characteristics across families of multi-body orbits that exist within this model —the Low-Thrust augmented Circular Restricted Three Body Problem (CRTBP-LT)— are exploited. The fidelity of the results from this algorithm is further expanded to an ephemeris model that includes the gravitational attraction of the Sun, the Earth and the Moon (SEM ephemeris model).

ADAPTIVE SLIDING ALGORITHM

The basic framework in the adaptive algorithm is identifying the intermediate arcs through which the vehicle 'slides' enroute to its destination. As a first step, assume that the goal is 'sliding' along a single family of orbits employing a low-thrust force to accomplish the corresponding energy change. The main goal of the reduced algorithm is, then, the construction of the minimum number of intermediate orbits through which to 'slide' from departure to destination.

Force Model: Low-Thrust Circular Restricted Three-Body Problem (CRTBP - LT)

The CRTBP is a time-invariant system in which two primary bodies –modeled as point masses– are assumed to be in coplanar and circular orbits relative to their barycenter, while a third body of negligible mass moves throughout the system[10,11]. The two primaries are labeled P_1 and P_2 with masses m_1 and m_2, respectively ($m_1 > m_2$); the equations of motion for the third-body, P_3 ($m_3 \ll m_1, m_2$), are derived from Newton's second law of motion for an inertial observer, and described in a frame that rotates about the system barycenter, where the z-axis is aligned with the angular momentum of the primary system, the x-axis is directed from P_1 to P_2, and the y-axis completes the right-handed triad.

Using the standard characteristic quantities to appropriately non-dimensionalize the system of equations, the characteristic length, $l^* = R_1 + R_2$, where R_1 and R_2 are the distances of the two primaries from the barycenter, respectively; the characteristic mass, $m^* = m_1 + m_2$; the characteristic time, $t^* = \sqrt{\frac{l^{*3}}{\tilde{G}m^*}}$, where $\tilde{G}$ corresponds to the universal gravitational constant. Let $n = 1$ be the non-dimensional angular velocity of the rotating frame with respect to the inertially fixed frame, and $\mu = \frac{m_2}{m_1+m_2}$ be the mass parameter of the system. If $\bar{x} = [x, y, z, \dot{x}, \dot{y}, \dot{z}, m]^T$ represents the non-dimensional state vector of P_3 with respect to the system barycenter, define the non-dimensional quantities $d = \sqrt{(x+\mu)^2 + y^2 + z^2}$ and $r = \sqrt{(x-1+\mu)^2 + y^2 + z^2}$ as the distances from P_3 to P_1 and P_2 respectively.

To incorporate the low-thrust acceleration of the spacecraft into the equations of motion, three control input parameters are introduced: a scalar quantity to represent the thrust magnitude, and two angles to orient the thrust vector. A pseudo-potential function is realized such that[12]:

$$U^*_{LT} = \frac{1-\mu}{d} + \frac{\mu}{r} + \frac{1}{2}\left(x^2 + y^2\right) + \bar{r} \cdot \bar{a}_T \tag{1}$$

where $\bar{a}_T = \frac{T}{m}\hat{a}_T$ represents the non-dimensional thrust acceleration vector; the unit vector $\hat{a}_T$ indicates the thrust direction, T corresponds to the non-dimensional thrust magnitude, $T = \tilde{T}\frac{t^{*2}}{m_3 l^* 1000}$, where $\tilde{T}$ is the dimensional thrust magnitude; and m is the non-dimensional mass of the spacecraft. The CRTBP-LT model is then evaluated as the following first-order system:

$$\begin{Bmatrix} \dot{\bar{r}} \\ \dot{\bar{v}} \\ \dot{m} \end{Bmatrix} = \begin{Bmatrix} \bar{v} \\ \bar{f}(\bar{r}, \bar{v}) + \frac{T}{m}\hat{a}_T \\ -\frac{T^2}{2\mathcal{P}} \end{Bmatrix} \tag{2}$$

If the specific impulse of the engine varies as time evolves, the mass rate of change with respect to time is denoted a Variable Specific Impulse model, or VSI. On the contrary, if the specific impulse remains fixed, the model is considered a Constant Specific Impulse engine, or CSI model. For the equations of motion described in Equations (2), a VSI model for the low-thrust spacecraft has been adopted for this investigation, where $\mathcal{P}$ represents the engine power.

Energy-Informed Optimization Algorithm

The proposed decision process for constructing sliding-type solutions in the CRTBP-LT model, is summarized in Figure 2. Note that the framework ultimately incorporates slides through any number of different families that are then stacked to reach a destination. To estimate the minimum number of intermediate orbits for 'sliding' enroute to the destination, the procedure relies on a parametrization of the energy evolution for the family in consideration, along with an accessible region —in configuration space— provided by the thrust capabilities of the spacecraft. This accessible region is denoted the Thrust Range Surface (TRS).

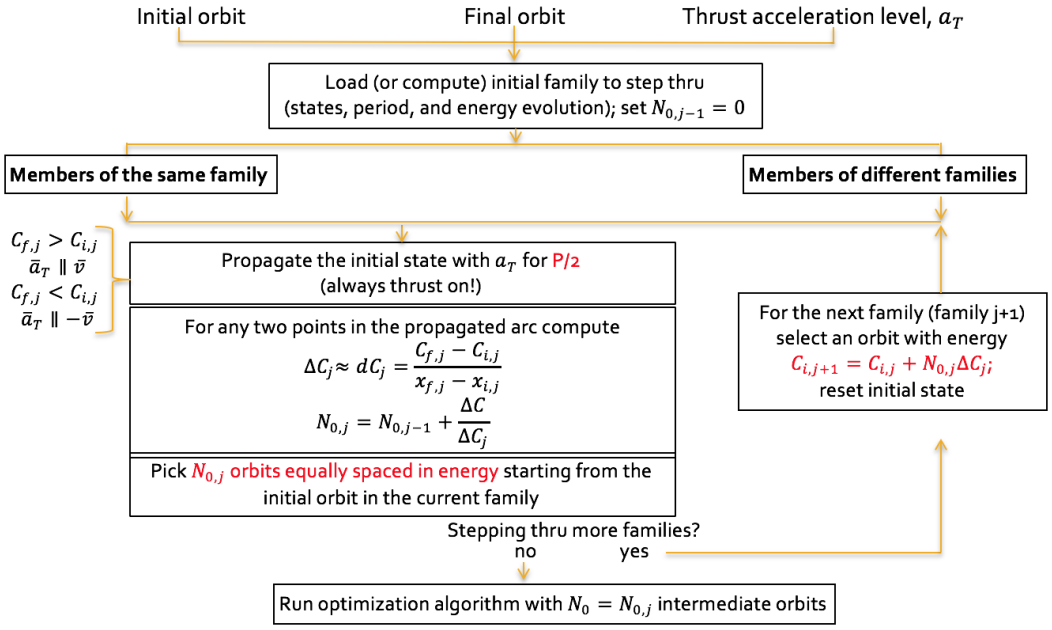

Figure 2. Energy-Informed Sliding Algorithm for Generation of Interior Trajectories

The algorithm is initialized by supplying three user-defined inputs: the departure and destination orbits as well as the maximum thrust acceleration level available due to the physical capabilities of the spacecraft. The output is a fully converged locally optimal transfer between the two orbits of interest. Furthermore, the solutions of this type do not depart the lunar vicinity (or some other bounded region in configuration space). The approach for constructing sliding-type geometry transfers is summarized, and visually represented, in the two steps described below, for a 14kg low-thrust spacecraft sample transfer from a L_2 Southern (S) Near Rectilinear Halo Orbit (NRHO) to a L_2 Northern (N) halo orbit, with a maximum thrust acceleration level consistent with that of the Lunar IceCube spacecraft, $8 \times 10^{-5} m/s^2$:

Step 1 Once the departure and arrival orbits are identified, as in Figure 3(a), the algorithm loads (or computes) a full representation of the families to which these orbits of interest belong. The capability does exist to represent additional families in the vicinity. For each family of interest, its representation in configuration space, as well as its period and energy evolution, are populated. While there exist multiple ways of parametrizing the energy evolution along a family of periodic orbits, the strategy in this algorithm employs a representation of the Jacobi constant evolution across the members of the family against the maximum and minimum x- coordinates for each orbit member as illustrated in Figure 3(b); this representation produces a surface denoted the Energy Surface (ES)

along the family, from which a limited grid search is conducted to select the intermediate orbits to serve as the initial guess for the transfer.

When the Energy Surface in Figure 3(b) exhibits monotonic growth (i.e., no extrema along the curve), this behavior indicates that no two orbits in the family possess the same value of Jacobi constant. Hence, once a direction of motion is identified, intermediate orbits for sliding are directly selected from the Energy Surface, either to increase or to decrease the energy to a value equal to that of the target orbit. When the Energy Surface exerts a non-monotonic growth (i.e., extrema along the curve), it suggests that the energy associated with each member of the family is no longer unique, and an extra step is required to identify the intermediate orbits best suited to slide through enroute to the destination orbit. This remark also suggests that the sliding direction across the family is not unique, i.e., there exist multiple ways to construct initial guesses for the sliding-type geometry.

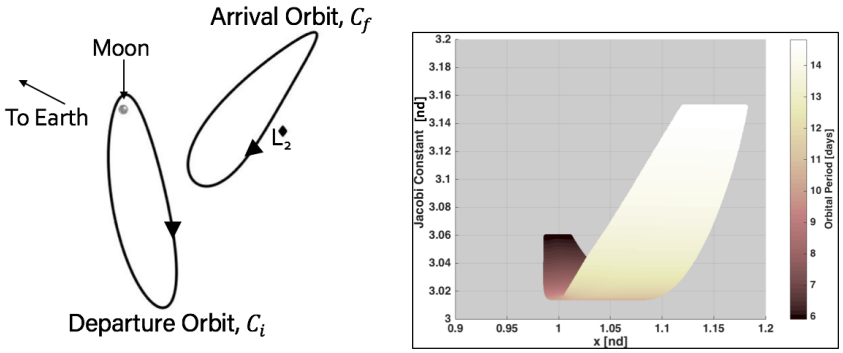

(a) Sample Departure and Arrival Orbits from the L_2 S and N Halo Families of Orbits

(b) Energy Surface for the L_2 S Halo Family

Figure 3. Energy Parametrization of the L_2 Southern (S) Halo Family

Two approaches for the selection of the intermediate orbits when energy is not unique, are explored in this investigation: 1. A Thrust Range Surface (TRS) (Figure 4), jumps along the Energy Surface, skipping the extrema in energy, and reducing the redundancies; 2. The algorithm decreases and/or increases energy in a non-monotonic fashion, by shifting the Energy Surface without skipping the extrema.

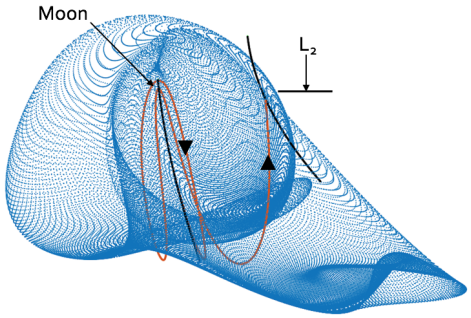

Figure 4. Thrust Range Surface for a L_2 Southern Near Rectilinear Halo Orbit (NRHO); TRS, Used to Skip Extrema along the Energy Surface

A Thrust Range Surface is a map in configuration space; the values of the components of the state vector are recorded at the end of a propagation segment that is initiated with the same set of initial conditions, but with only the thrust direction modified for each outcome. This surface supplies initial guesses for arcs that do not slide incrementally through the family, rather arcs that are jumping along

the Energy Surface to a value for which the selection of the orbit ultimately becomes unique. The shape and reach of a Thrust Range Surface is a function of the acceleration magnitude as well as the orbit being examined.

Step 2 To generate a converged locally optimal solution, the strategy then involves the formulation of an energy-informed minimization problem. The goal is the determination of the minimum number of intermediate orbits, N, that minimizes the following cost function:

$$J = \min_{N \in \mathbb{N}} \left\{ \left[W_1 \left(\frac{1}{2} \sum_{j=1}^{N} \Delta C_j^2 \right) \right] - [W_2 ToF] \right\} \tag{3}$$

where C_j represents the energy of each intermediate orbit as reflected in the corresponding value of the Jacobi constat, and ToF is the total time-of-flight along the transfer. This nondimensional objective function is comprised of two different terms: (i) an energy related term, whose main purpose is the reduction of the number of energy changes from one propagation arc along the transfer to the next; such a minimization is accomplished by means of a mass-optimal solution; and (ii) a time-of-flight term, included in the objective function to accommodate time-optimal trajectories. The weights associated with each of the individual terms are represented by $W_{1,2}$, respectively, and aid in prioritizing the type of optimal transfer to be delivered. The problem formulation then requires an initial guess for the optimal number of intermediates orbits, N_0, as well as for the change of energy per orbit, ΔC_{j0}.

To generate mass locally optimal transfers with a sliding-type geometry, the sliding algorithm solves the minimization problem in Equation (3), by initially assigning $W_1 = 1$ and $W_2 = 0$. From the initial guess, a feasible solution is first generated by means of a multiple-shooting differential corrections scheme that discretizes each intermediate orbit into patch points and segments (each of which is allowed to thrust or coast over the duration of the arc); The discretization scheme allows n total points and $n-1$ total segments, as illustrated in Figure 5, where $\bar{x}_j$ represents the state vector for each segment j, and the control variables required per arc segment are identified. The orientation of the thrust vector is defined by the control angles α and β that correspond to the in-plane and out-of-plane angles, respectively, and orient the thrust acceleration vector in the barycentric rotating frame. The algorithm employs a turn-and-hold control logic, such that the same thrust magnitude and orientation are fixed over the duration of each thrust/coast arc.

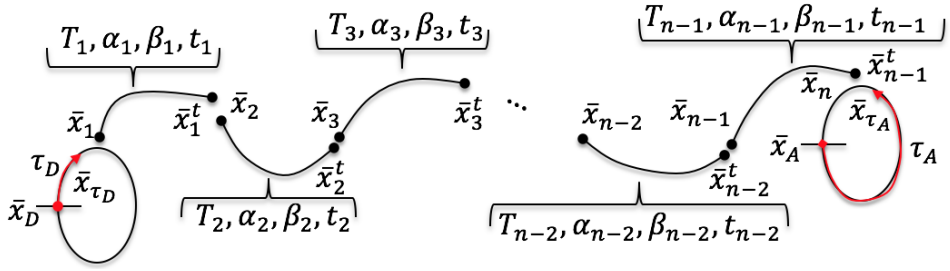

Figure 5. Illustration of a Multiple Shooting Differential Corrections Strategy

Corrections Algorithm. The corrections process is implemented via a multiple-shooting scheme, one that seeks to generate a feasible solution that is continuous in the position, velocity and mass states. This multiple-shooting approach determines a solution by employing a multi-dimensional iterative Newton strategy, in which the update equation is based on the minimum norm solution as:

$$\bar{X}_{j+1} = \bar{X}_j - DF(\bar{X}_j)^T \left[DF(\bar{X}_j)DF(\bar{X}_j)^T\right]^T \bar{F}(\bar{X}_j) \tag{4}$$

where $\bar{X}_j$ represents the vector of free variables —or controls— as in Figure 5, $\bar{F}(\bar{X}_j)$ corresponds to the vector of constraints, and $DF(\bar{X}_j)$ is the Jacobian matrix comprised of the partial derivatives of the constraints with respect to the free variables. Furthermore, all inequality constraints are converted into equality constraints via the use of slack variables, such that those constraints are also included in the vector $\bar{F}(\bar{X}_j)$[13]. This conversion impacts the dimensionality of the problem, as each slack variable is also added to the vector of free variables, $\bar{X}_j$, as follows:

$$\begin{aligned} T_i - T_{max}\sin^2(\eta_{T_i}) = 0 \quad &, \quad t_i - \eta_{t_i} = 0 \\ \alpha_i - 2\pi\sin^2(\eta_{\alpha_i}) = 0 \quad &, \quad \beta_i - \pi\sin^2(\eta_{\beta_i}) = 0 \\ \tau_D - \mathbb{P}_D\sin^2(\eta_{\tau_D}) = 0 \quad &, \quad \tau_A - \mathbb{P}_A\sin^2(\eta_{\tau_A}) = 0 \end{aligned} \tag{5}$$

where η_{T_i}, corresponds to the slack variable related to the thrust magnitude for arc i; η_{t_i} is the slack variable associated with the integration time along segment i; η_{α_i} and η_{β_i} are the slack variables related to the thrust orientation vector along the i^{th} arc; η_{τ_D} and η_{τ_A} correspond to the slack variables associated with the time-like parameters, τ_D and τ_A, that represent the coast segments along the departure and arrival orbits[14]; and, finally, the variables $\mathbb{P}_D$ and $\mathbb{P}_A$ are evaluated as the orbital period of the departure and arrival orbits, respectively.

The Jacobian matrix, $DF(\bar{X}_j) = \frac{\partial F(\bar{X}_j)}{\partial \bar{X}_j}$, is constructed either analytically or via finite difference numerical derivatives. Once a feasible solution is generated, it serves as an initial guess for a direct optimization procedure as implemented in MATLAB's fmincon optimization function. The objective is the minimization of the performance function specified in Equation (3), subject to:

$$\begin{aligned} \text{the differential constraints} \quad & \ddot{x} = 2\dot{y} + U_x^* + \frac{T}{m}cos\left(\alpha\right)cos\left(\beta\right) \\ & \ddot{y} = -2\dot{x} + U_y^* + \frac{T}{m}sin\left(\alpha\right)cos\left(\beta\right) \\ & \ddot{z} = U_z^* + \frac{T}{m}sin\left(\beta\right) \\ & \dot{m} = -\frac{T^2}{2P} \\ \text{the prescribed conditions} \quad & \bar{x}_0 = \bar{x}_D, m_0 = 1, t_0 = 0, N_0, \bar{x}_n = \bar{x}_{\tau_A} \\ \text{the inequality constraints} \quad & 0 \leq T_1 \cdots T_{n-1} \leq T_{max}, t_1 \cdots t_{n-1} > 0 \\ & 0 \leq \alpha_1 \cdots \alpha_{n-1} \leq 2\pi, \ -\pi/2 \leq \beta_1 \cdots \beta_{n-1} \leq \pi/2 \\ & 0 \leq \tau_D \leq \mathbb{P}_D, 0 \leq \tau_A \leq \mathbb{P}_A \\ \text{and the path constraints} \quad & \bar{x}_1 = \bar{x}_{\tau_D}, \bar{x}_2 = \bar{x}_1^t, \ \cdots, \bar{x}_n = \bar{x}_{n-1}^t \end{aligned} \tag{6}$$

where $\bar{x}_j$ (for $j = 1, .., n$). Recall that these $\bar{x}_j$ correspond to the states at the beginning of each arc segment, and $\bar{x}_j^t$ represent the states at the termination point on that particular segment. To ensure that the spacecraft departs and arrives at the specified destination and arrival orbits, two time-like parameters, τ_D and τ_A, are introduced into the multiple shooting algorithm as additional constraint variables to enforce coast arcs along the orbits of interest. Note that, in this strategy, τ_D is propagated forward in time, while τ_A is propagated backwards on the destination orbit.

ENERGY-INFORMED INITIAL GUESS GENERATION

The initial guess estimate for the minimum number of intermediate orbits, N_0, that are required for sliding-type transfers between cislunar orbits that exist within the same family in the CRTBP model, is accomplished by leveraging the Jacobi constant of integration. For any particular transfer, once the departure and arrival orbits are identified, the total net energy change to accomplish the transfer is deduced from the simple relationship:

$$\Delta C = C_{departure} - C_{arrival} = C_i - C_f$$

where $C_i = C_{departure}$ is the energy of the initial/departure orbit, and $C_f = C_{arrival}$ corresponds to the energy of the final/destination orbit. Furthermore, the energy of the arrival orbit is decomposed in terms of the change in energy between each pair of intermediate orbits as follows:

$$C_f = C_i + \sum_{j=1}^{N} \Delta C_j \tag{7}$$

To determine the initial direction of motion along the energy surface in Figure 3(b), i.e., the initial orientation of the thrust vector, the following logic is implemented:

$$\begin{cases} \bar{a}_T \| \bar{v} & \text{if } C_{f,j} < C_{i,j} \\ \bar{a}_T \| -\bar{v} & \text{if } C_{f,j} > C_{i,j} \end{cases}$$

If $C_{i,j}$ represents the energy of the current intermediate orbit, and $C_{f,j}$ is the energy of the next intermediate orbit, the algorithm induces thrust along the relative velocity direction whether or not an increase in energy is desired per Equation (7). Once the initial thrust arc is propagated for a fixed duration, the algorithm evaluates a linear approximation for the initial change in energy per orbit as described in Figure 6(a), and employs this approximation to estimate an initial guess for the number of intermediate orbits. This process is represented graphically as described in Figure 6(b), and computed numerically as follows:

$$\Delta C_{j0} \approx dC_j = \frac{C_{f,j} - C_{i,j}}{x_{f,j} - x_{i,j}} \tag{8}$$

$$N_{0,j} = \frac{\Delta C}{\Delta C_{j0}} \tag{9}$$

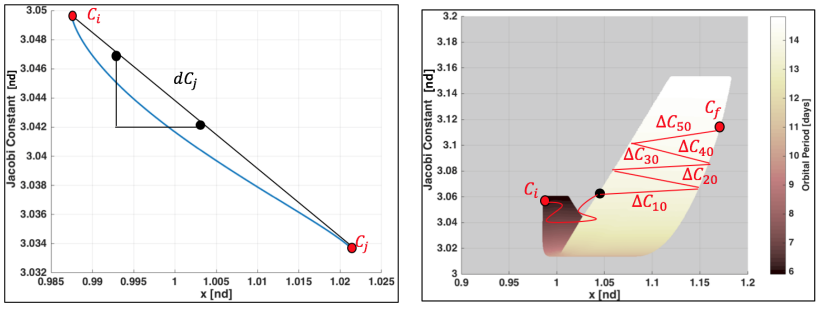

(a) Linear Approximation of Energy Change due to Maximum Thrust Acceleration Magnitude

(b) Initial Estimate for Number of Intermediate Orbits in the L_2 S Halo Energy Space

Figure 6. Visual Representation of the Energy-Informed Initial Guess Generation Process

As indicated in the diagram in Figure 2, the process continues for each family that is incorporated into the construction of a particular initial guess for a transfer with a sliding-type geometry. For the sample scenario being examined, a visual representation of the initial guess in configuration space is illustrated in Figure 7(a). The algorithm then utilizes a direct optimization process via a multiple-shooting approach, as described in the previous section, to generate the optimal solution in the CRTBP-LT model in Figure 7(b).

To produce this solution, the sliding algorithm employs two intermediate orbits —one member of the southern halo family and one member of the nothern halo family— combined with the TRS generated for the departure orbit, while guaranteeing that the constraint on the maximum thrust acceleration magnitude is not violated. To further evaluate the accuracy and robustness of the adaptive sliding algorithm, all results are transitioned to a higher-fidelity ephemeris force model.

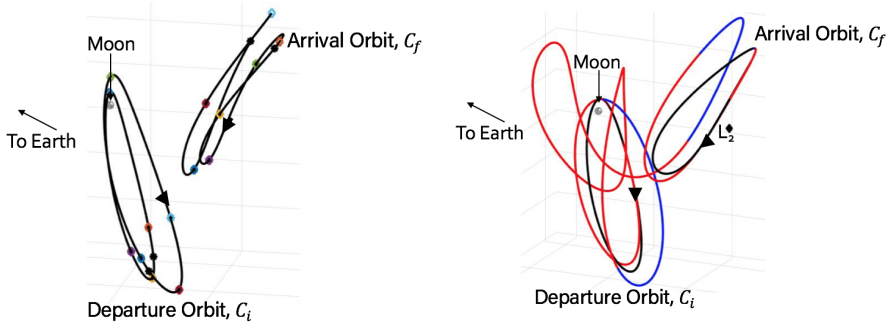

(a) Initial Guess from the Sliding Algorithm (b) Mass Optimal Converged Solution

Figure 7. Sample Transfer Scenario from a L_2 S NRHO to a L_2 N Halo Orbit in the CRTBP-LT Model via Sliding Algorithm. Red and blue arcs represent thrust and coast arcs, respectively

Force Model: Low-Thrust *n*-Body Ephemeris Model

The assumptions under the circular restricted three-body problem are usually sufficient for the purposes of preliminary analysis and mission design; however, in reality, the spacecraft, P_3, is moving in a time-dependent system under perturbations from the gravitational effects of other celestial bodies[9,10]. To better represent this motion, the acceleration of the spacecraft with respect to a primary body, under the gravitational influence of n additional nearby bodies, is derived, where all coordinates are expressed in a J2000 inertial reference frame centered on the primary body, as follows:

$$\ddot{\bar{r}}_{q3} = -\frac{\tilde{G}\left(M_3 + M_q\right)}{r_{q3}^3}\bar{r}_{q3}^3 + \tilde{G}\sum_{j=1, j\neq q,3}^{n} M_j\left(\frac{\bar{r}_{3j}}{r_{3j}^3} - \frac{\bar{r}_{qj}}{r_{qj}^3}\right) + \frac{\tilde{T}}{M}\hat{a}_T \tag{10}$$

Let $\tilde{T}$ represent the dimensional thrust acceleration level, M corresponds to the dimensional mass of the spacecraft, M_j is the dimensional mass of each perturbing body, and $\tilde{G}$ is the dimensional gravitational constant. Furthermore, since the system of equations is no longer time-invariant, time epochs emerge as an important component of the transfer design, for which ephemerides deliver the precise locations of all bodies at each specified point in time. In the particular model in Equation (10), all celestial bodies are modeled as point masses such that perturbations due to J_2 effects, other spherical harmonics, drag, and/or and solar radiation pressure are not incorporated in this model at this time.

There exist multiple strategies to transition a sliding solution from the CRTBP-LT to the ephemeris model[15], two of which are explored in this investigation. Strategy I: using the sliding algorithm, generate a converged locally optimal trajectory in the CRTBP-LT model; transition the full solution to ephemeris by transforming each position, velocity, and thrust orientation state from rotating to inertial coordinates; correct —and possibly optimize— in the ephemeris model. The transfer in Figure 8(a) is a locally optimal solution generated from the sliding algorithm in the CRTBP-LT model. Strategy I dictates that this transfer be transformed into inertial coordinates, and later re-converged using a higher-fidelity ephemeris model, with a goal that the transfer geometry be generally preserved, as illustrated in Figure 8(b).

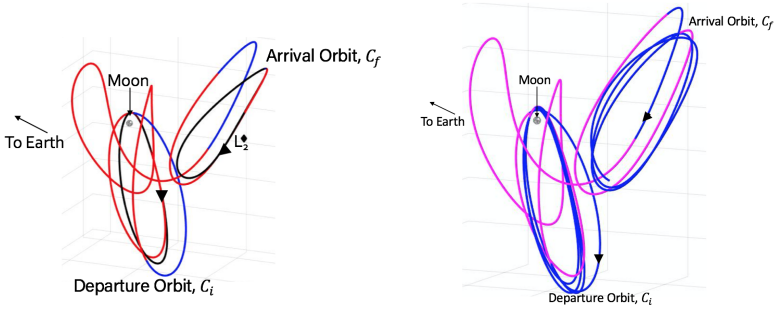

(a) L_2 S NRHO to L_2 N Halo Transfer in the CRTBP-LT via Sliding Algorithm

(b) L_2 S NRHO to L_2 N Halo Transfer in the Ephemeris Model via Strategy I

Figure 8. Strategy I for Constructing Sliding Geometry Transfers in the Ephemeris Model. Red and Blue Arcs Represent Thrust and Coast Segments in the CTRBP-LT model; Magenta and Cyan correspond to Thrust and Coast Segments in the Ephemeris Model

Strategy II: using the sliding algorithm, populate the initial guess for the minimum number of intermediate orbits necessary to slide through the family from the departure to the destination orbit; transform the position and velocity states for each intermediate periodic orbit into inertial coordinates; specify the thrust orientation vector control law with inertial pointing; correct —and possibly optimize— in the ephemeris model. Figure 9(a) is a visual representation of the initial guess that is generated by the sliding algorithm, describing the minimum number of intermediate orbits to accomplish the transfer. Transitioning these individual periodic orbits into the ephemeris model and, then, using a corrections algorithm to compute a converged trajectory, is the procedure from Strategy II that produces the path in Figure 9(b).

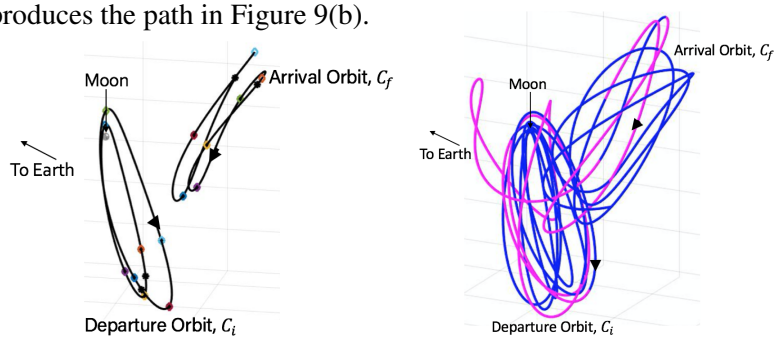

(a) L_2 S NRHO to L_2 N Halo Initial Guess in the CRTBP-LT from Sliding Algorithm

(b) L_2 S NRHO to L_2 N Halo Transfer in the Ephemeris Model via Strategy II

Figure 9. Strategy II for Constructing Sliding Geometry Transfers in the Ephemeris Model. Magenta and Cyan correspond to Thrust and Coast Segments in the Ephemeris Model

The ephemeris trajectory in Figure 8(b) preserves the geometry of the CRTBP-LT transfer utilized as initial guess in Strategy I; whereas, the ephemeris path in Figure 9(b), include multiple revolutions of each intermediate CRTBP orbit member, generated by the sliding algorithm in the construction of the initial guess for Strategy II. Thus, the time-of-flight required for the spacecraft to travel from the departure to the arrival orbit in Strategy II, 164.7831 days, is larger than the travel time required in Strategy I, of 50.3245 days.

Regardless of the strategy, converging a trajectory in the ephemeris model is an epoch dependent problem. Depending on the position of the Sun as well as the other perturbing bodies added to the model at a specific epoch, the sensitivity of the problem might change, causing the corrections algorithm to increase the number of iterations to produce a converged solution. To alleviate convergence issues based on epoch dependencies, the concept of a roughness parameter is implemented to increase the probability of convergence for a particular epoch.

Roughness Parameter

The roughness parameter is a mathematical artifact employed in many fields of science to quantify the smoothness of a curve[16]. These parameters are categorized in three main groups: (i) amplitude parameters, which measure the vertical characteristics of the profile; (ii) spacing parameters that measure the horizontal characteristics of the profile; (iii) and the hybrid parameters, described as a combination of amplitude and spacing parameters. One of the most popular definitions for amplitude parameters is the Root Mean Square value (RMS), that is,

$$R_{ms} = \sqrt{\frac{1}{k}\sum_{i=1}^{k} p_i^2} \tag{11}$$

where k represents the number of points in the profile, and p_i corresponds to the parameter of interest at point i. In this investigation, the RMS roughness parameter definition is utilized to estimate the most suitable epoch to transition a solution from the CRTBP-LT to the ephemeris model, based on the 'true' location of the celestial bodies included in the equations of motion. In addition, a specified number of revolutions of the initial and final orbits are stacked and added as additional arcs to the beginning and end of the trajectory, respectively, to guarantee departure and arrival from suitable orbits in the higher fidelity model.

A Roughness Parameter Map (RPM) is then populated by parametrizing a number of stacked revolutions along the departure and arrival orbits against a variety of different epochs. The parameters of interest are the position and velocity states along the CRTBP-LT trajectory as transformed into inertial coordinates, and their respective RMS value is stored on the map. In summary, to transition a sliding geometry trajectory into the ephemeris model employ the following steps:

1. Stack a specified number of revolutions on the initial and final orbits in the CRTBP-LT model
2. For a variety of epochs (e.g., each month within a year, or each day within a month), transform the CRTBP-LT position, velocity and thrust orientation vector states into inertial coordinates
3. Populate the initial guess for the inertial trajectory at each epoch in Step 2
4. Compute the RMS values along the trajectory in Step 3 over all selected epochs in Step 2. These values are stored in a map, denoted the Roughness Parameters Map (RPM)

5. Use the RPM to select the epoch with the lowest RMS value; and then the corrections algorithm converges this initial guess for the selected epoch in the ephemeris model

6. If a specific epoch is desired for the ephemeris trajectory, apply a natural parameter continuation process on the epoch converged in Step 5, to re-converge the solution until the specified epoch is achieved

The adaptive sliding algorithm in the CRTBP-LT model is employed to generate a variety of transfers in the cislunar region that, combined with the RPM procedure, generates higher-fidelity sliding geometry solutions. Two sample mission applications are successful in accomplishing the goal.

Application: Mass-Optimal Transfer from a L_2 Southern (S) NRHO to a L_2 Northern (N) NRHO

To illustrate the performance of the sliding algorithm, consider a sliding-type low-thrust transfer for a 14 kg spacecraft with a maximum acceleration level of $8 \times 10^{-5} m/s^2$, from a L_2 Southern Near Rectilinear Halo Orbit (NRHO) with energy $JC = 3.0553$ to a L_2 Northern NRHO with energy $JC = 3.0441$ in the Earth-Moon CRTBP-LT system. The energy parametrization for both families of interest appears in Figures 10(a)-(c) and 11(a)-(c), respectively.

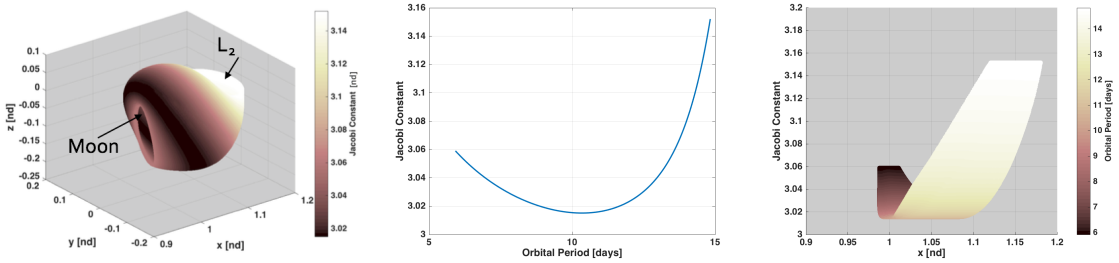

(a) L_2 S Halo Configuration Space (b) L_2 S Halo Energy Evolution (c) L_2 S Halo Energy Surface

Figure 10. Energy Parametrization for the L_2 S Halo Families of Orbits

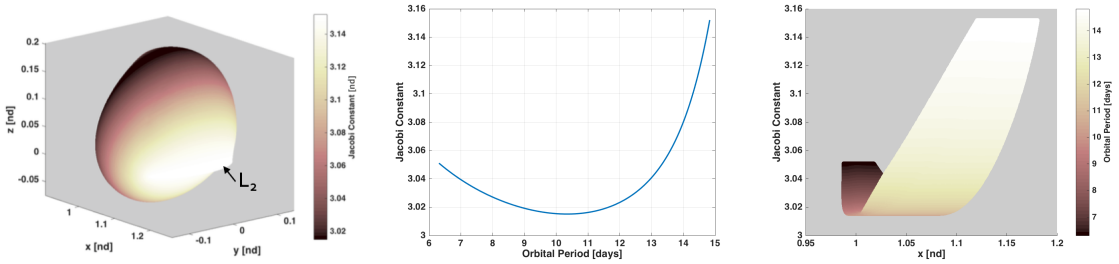

(a) L_2 N Halo Configuration Space (b) L_2 N Halo Energy Evolution (c) L_2 N Halo Energy Surface

Figure 11. Energy Parametrization for the L_2 N Halo Families of Orbits

The initial guess generated from the sliding algorithm in the CRTBP-LT model for this transfer is plotted in Figure 12(a), while the converged solution, in the same force model, appears in Figure 12(b); the energy and thrust acceleration evolution for the converged solution are represented in Figure 12(d), while the corresponding trajectories in different views of the Sun-Earth-Moon (SEM) ephemeris model are depicted in Figures 13(b)-(d). Blue and red arcs correspond to coast and thrust arcs in the CRTBP-LT model, whereas cyan and magenta arcs represent coast and thrust segments in the SEM ephemeris model, respectively.

The trajectory is transitioned to the ephemeris model for September 1, 2021; this epoch is selected from the RPM generated via Strategy I as illustrated in Figure13(a). In the CRTBP-LT model, the spacecraft requires 72.9701 days from the time it departs the original orbit (represented in Figure 12 as the first thrusting arc) until arrival on the destination orbit (i.e., the last thrusting arc). The transfer path requires about 0.0461kg (0.3335%) of the 14kg initial mass, which corresponds to an equivalent ΔV of $81.8931 m/s$. In the ephemeris model, for this particular epoch, the equivalent ΔV consumption increases to $103.1541 m/s$ or 0.0588kg of the initial spacecraft mass, while the time-of-flight is reduced to 72.6896 days. Note that, since the performance in the ephemeris model is epoch dependent, the ΔV consumption is modified by re-converging this locally mass-optimal solution for a different time epoch.

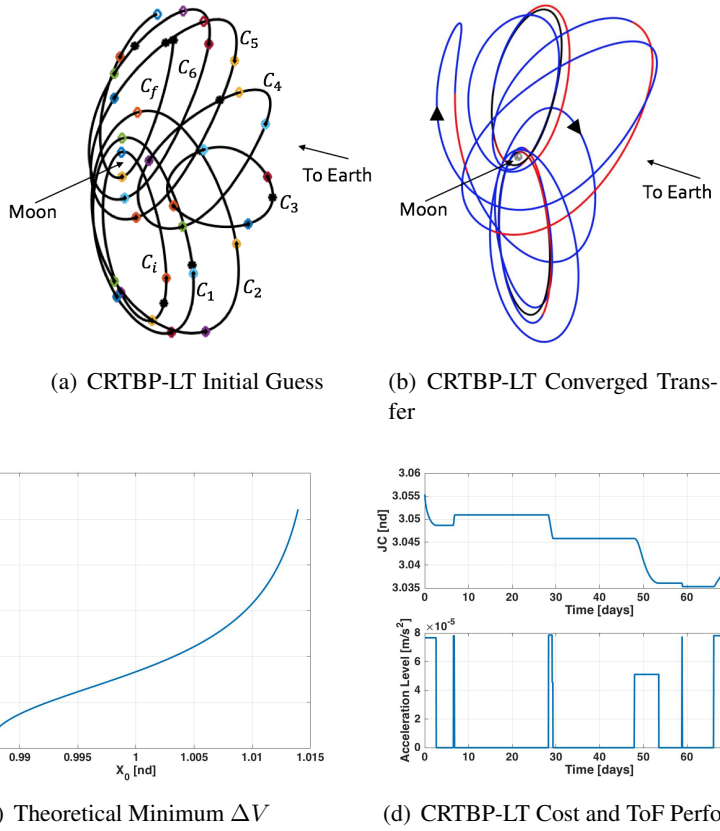

(a) CRTBP-LT Initial Guess

(b) CRTBP-LT Converged Transfer

(c) Theoretical Minimum ΔV

(d) CRTBP-LT Cost and ToF Performance

Figure 12. Performance for a Mass Optimal LT Transfer from a L_2 S NRHO to a L_2 N NRHO in the CRTBP-LT Model

To assess the performance of the solution, the propellant consumption is compared with the theoretical minimum ΔV estimated for this transfer[14], as illustrated in Figure 12(c). In terms of propellant consumption, note that the sliding algorithm produces a path more costly than the theoretical minimum. However, there exists a trade-off between reducing propellant cost, and producing a trajectory that, despite the highly dynamically sensitive region of space —such as the cislunar region— the spacecraft remains within the vicinity of the Moon over the entire duration of the transfer. Moreover, the sliding algorithm produces transfers leveraging the dynamical environment, even though the departure and arrival orbits are stable in the Lyapunov sense, i.e., they do not possess arcs that naturally depart and/or approach the periodic orbit.

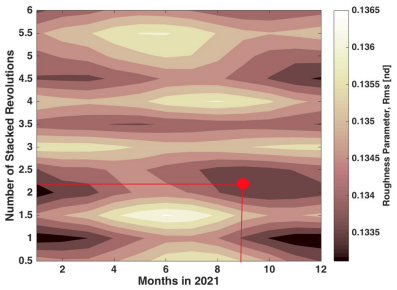

(a) RPM

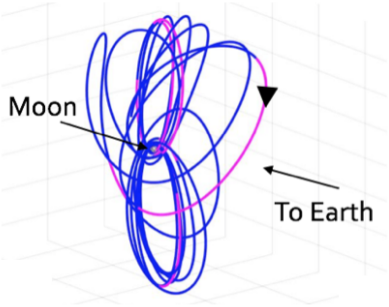

(b) J2000 Moon-Centered Ephemeris

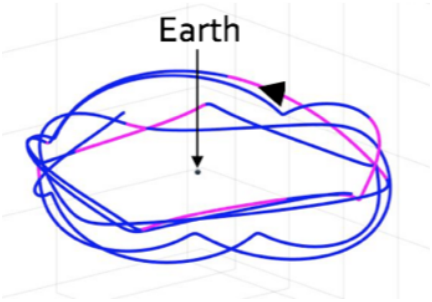

(c) Earth-Centered Ecliptic Ephemeris

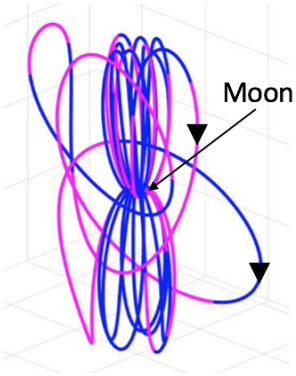

(d) Moon-Centered Ecliptic Ephemeris

Figure 13. Performance for a Mass Optimal LT Transfer from a L_2 S NRHO to a L_2 N NRHO in the SEM Ephemeris Model

Application: Mass-Optimal Transfer from a L_2 Lyapunov to a L_2 Vertical Orbit

Consider the design of a low-thrust transfer with a sliding-type geometry for a 500 kg spacecraft from a L_2 Lyapunov orbit with the energy level $JC = 3.0001$ to an L_2 vertical orbit with energy $JC = 2.7172$ in the Earth-Moon CRTBP system, with a maximum thrust acceleration level of $4 \times 10^{-4} m/s^2$. The biggest challenge when designing this transfer is the large change in the inclination between the two families; thus, it is beneficial to leverage one or more orbits from an intermediate family to gradually alter the inclination of each intermediate orbit and, thus, accomplish the sliding type transfer. Based on the evolution of each member of the L_2 axial family depicted in Figure 14, its energy span, and its 'reach' in z-amplitude, this additional family is selected for inclusion. Note that the selection of an intermediate family is arbitrary. However, an informed choice is beneficial.

The inputs to the sliding algorithm are the departure and arrival orbits, the maximum thrust acceleration level allowed by the spacecraft, and the inclusion of the L_2 axial family as intermediate orbit members. As apparent in Figure 15, the algorithm proceeds to generate the energy parametrization for each of the individual families, as this parametrization is the key factor for later selection of the individual L_2 axial orbits to incorporate as the intermediate arcs along the transfer.

The initial guess generated by the sliding algorithm is plotted in Figure 16(a); the algorithm selects one orbit from the Lyapunov family —the departure orbit—, one orbit form the vertical family

—the arrival orbit—, and six orbits from the axial family. The converged solution in the CRTBP-LT model is depicted in Figure 16(b). As expected, the final transfer resembles the geometry of the initial guess, where blue and red arcs represent coast and thrust arcs in the CRTBP-LT model; the energy evolution and the thrust acceleration levels in the converged solution in the CRTBP-LT model are detailed in Figure 16(d). In this model, the spacecraft requires 132.9845 days from the time of departure from the initial orbit (represented in Figures 16 as the first thrusting arc) until the time it arrives on the destination orbit (i.e., the last thrusting arc). In this model, the spacecraft arrives at its final destination with 99.1754% of its initial mass, thus, only 0.8246kg of the 500kg initial mass was expended for the transfer. Converting this performance to an equivalent ΔV results in $324.7892m/s$ of propellant consumption, which is within the range of the theoretical minimum ΔV required for motion from the departure to the destination orbits represented in Figure 16(c).

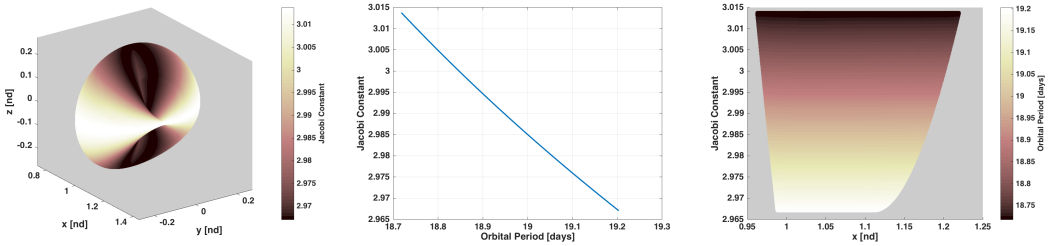

(a) L_2 Axial Configuration Space (b) L_2 Axial Energy Evolution (c) L_2 Axial Energy Surface

Figure 14. Energy Parametrization for the L_2 Axial Family

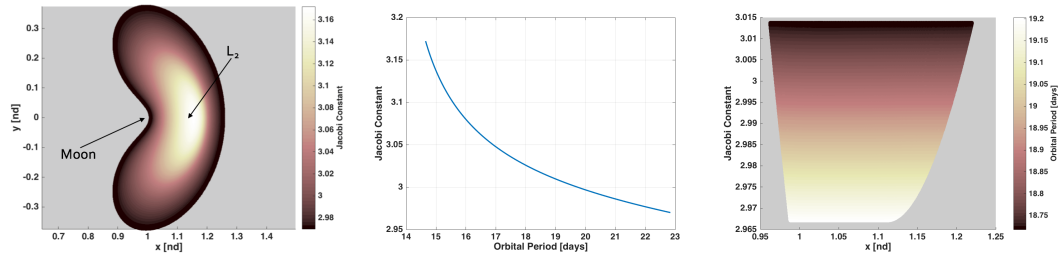

(a) L_2 Lyapunov Configuration Space (b) L_2 Lyapunov Energy Evolution (c) L_2 Lyapunov Energy Surface

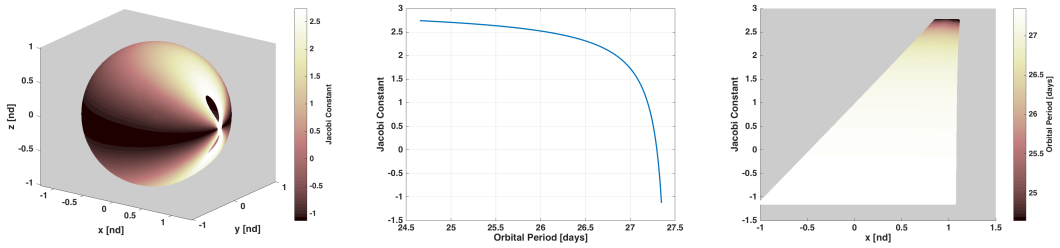

(d) L_2 Vertical Configuration Space (e) L_2 Vertical Energy Evolution (f) L_2 Vertical Energy Surface

Figure 15. Energy Parametrization for the L_2 Lyapunov and L_2 Vertical Families

Transitioning the converged solution into the ephemeris model, as illustrated in Figures 17(b)-(d) for March 1, 2021, recall that cyan and magenta segments correspond to coast and thrust arcs, respectively. The epoch is selected based on the RPM illustrated in Figure 17(a). For this particular epoch in the ephemeris model, the equivalent ΔV consumption is reduced to $292.6643m/s$, that

corresponds to 0.9981% of the 500kg initial mass, while the total time-of-flight required is 117.7946 days.

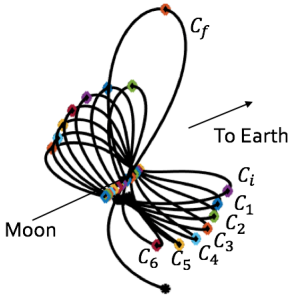

(a) CRTBP-LT Initial Guess

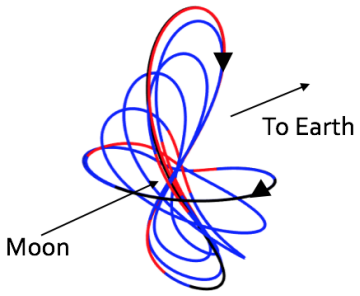

(b) CRTBP-LT Converged Transfer

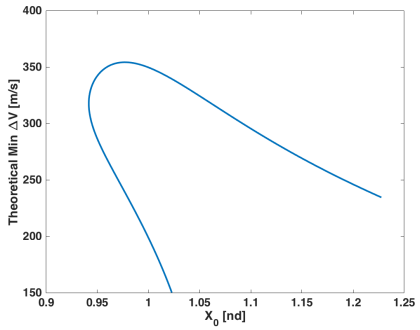

(c) Theoretical Minimum ΔV

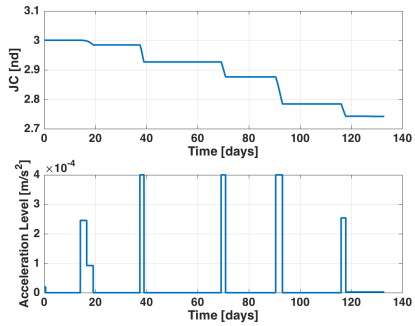

(d) CRTBP-LT Cost and ToF Performance

Figure 16. Performance for a Mass Optimal LT Transfer from a L_2 Lyapunov to a L_2 Vertical via L_2 Axial in the CRTBP-LT Model

Application: Time-Optimal Transfer from a L_2 Lyapunov to a L_2 Vertical Orbit

As a final sample application, consider re-designing the low-thrust transfer for a 500 kg spacecraft from a $JC = 3.0001$ L_2 Lyapunov orbit to a $JC = 2.7172$ L_2 vertical orbit in the Earth-Moon CRTBP system, as a time-optimal solution. The adaptive sliding algorithm proceeds to modify the weights on the objective function in Equation (3), such that priority is shifted to the time-of-flight minimization term.

To initiate the design, the process uses the initial guess illustrated in Figure 16(a). The converged time-optimal solution produced by the adaptive sliding algorithm is plotted in Figure 18(a), while the energy and time-of-flight evolutions are represented in Figure 18(b). Comparing these two locally optimal solutions (i.e., the mass-optimal solution in Figures 16 and the time-optimal solution in Figures 18), the time-of-flight required for the spacecraft from departure to destination is reduced from 132.9845 days to 11.6653 days from the mass-optimal to the time-optimal solution; the propellant consumption, however, increases from 0.9981% to 1.0277% of the 500kg initial mass, that, in terms of equivalent ΔV, indicates that the mass consumption increases from $324.7892m/s$ in the mass-optimal case to $405.2372m/s$ in the time-optimal solution. These performances suggest that for this particular application, the time-optimal solution offers a suitable trade-off between transfer time and propellant cost benefits, as the penalty in increasing the cost is largely overshadowed by the reduction in travel time.

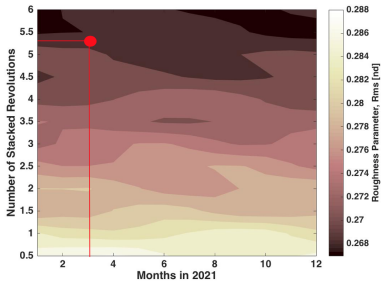

(a) RPM

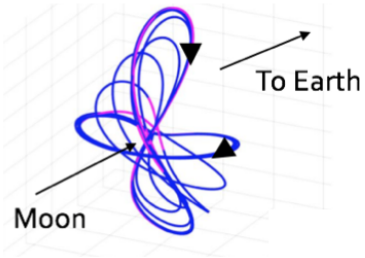

(b) J2000 Moon-Centered Ephemeris

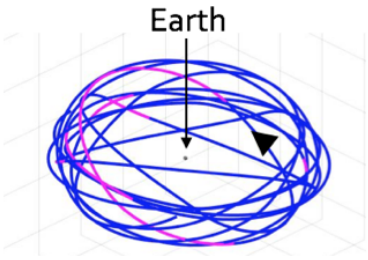

(c) Earth-Centered Ecliptic Ephemeris

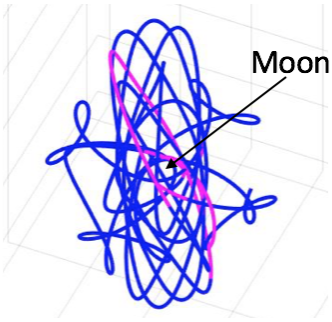

(d) Moon-Centered Ecliptic Ephemeris

Figure 17. Performance for a Mass Optimal LT Transfer from a L_2 Lyapunov to a L_2 Vertical via L_2 Axial in the SEM Ephemeris Model

As a result of maintaining active thrusters over the entire duration of the trajectory, the energy evolution for the time-optimal transfer in Figure 18(b) is a smooth curve; alternatively, the energy evolution of the mass-optimal trajectory in Figure 16(d) exerts a staircase-like behaviour, reflecting the spacecraft passage through each intermediate orbit, to gradually accomplish the large change in inclination required to transition from a planar to a spatial orbit, while ensuring the least locally possible propellant consumption.

These time-optimal results are further examined via a natural parameter continuation procedure on the maximum thrust acceleration level experienced by the spacecraft[14], to produce a family of minimum time-of-flight solutions from departure to arrival orbit, as illustrated in Figure 19(a). As the maximum thrust acceleration level is gradually decreased from $4 \times 10^{-4} m/s^2$ to $2 \times 10^{-4} m/s^2$, an acceleration level consistent with that of the DAWN spacecraft[4], a new path is constructed by the adaptive sliding algorithm, and its representation in configuration space in plotted as a new lighter shade of the darker red trajectory in Figure 19(a). Moreover, the time-of-flight and the equivalent ΔV performance for each trajectory are depicted in Figure 19(b), where it is apparent that as the thrust acceleration level decreases, the time-of-flight of the time-optimal solution generally increases, as well as the equivalent ΔV.

The results from the time-optimal solutions in Figures 19 are coherent within the context of the expected behaviour of the low-thrust spacecraft[17,18]. If all other parameters remain fixed (e.g., departure and destination orbit, and engine specific impulse), the smaller the thrust acceleration level, the greater the time interval required for the vehicle to navigate the same region in space, and the more propellant-expensive the transfer.

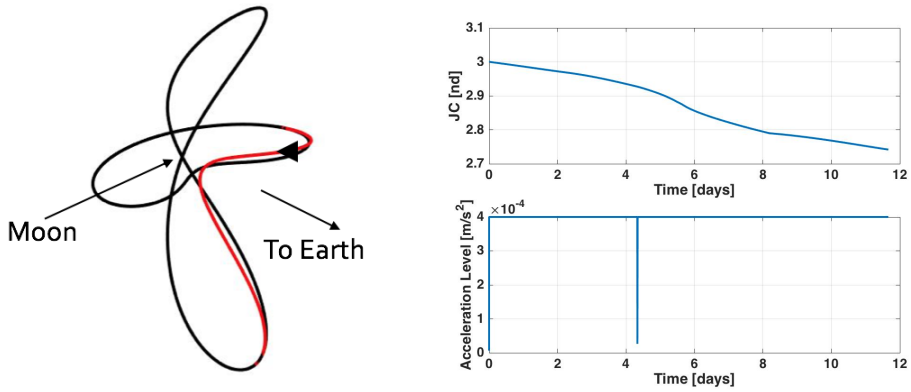

(a) CRTBP-LT Converged Solution (b) CRTBP-LT Cost and ToF Performance

Figure 18. Performance for a Time Optimal LT Transfer from a $JC = 3.0001$ L_2 Lyapunov to a $JC = 2.7172$ L_2 Vertical in the CRTBP-LT Model. Red represents thrust arcs

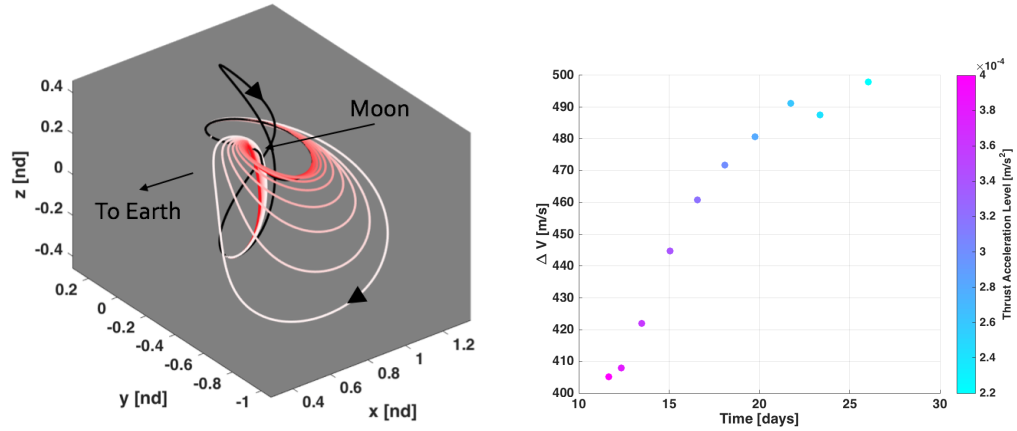

(a) CRTBP-LT Time-Optimal Family of Solutions (b) CRTBP-LT Cost and ToF Performances

Figure 19. Performance for a Time Optimal Family of LT Transfers from a $JC = 3.0001$ L_2 Lyapunov to a $JC = 2.7172$ L_2 Vertical in the CRTBP-LT Model

CONCLUDING REMARKS

The adaptive sliding algorithm successfully produces transfers over a range of low-thrust problems of varying complexity. While manifold arcs aid in constructing interior and exterior transfer geometries, the energy-informed adaptive sliding algorithm offers the capability for identifying interior transfer geometries when manifolds arcs are not available, e.g., when moving between stable periodic orbits. Furthermore, the sliding methodology is valid for any CRTBP-LT model, and employs members of different families as intermediate orbits, consistent with an orbit chaining method. Since the geometry of the converged solution relies heavily on the initial guess, there are an infinite number of options for sliding through a bounded region of space and transferring between departure and arrival orbits.

Trajectories resulting from this algorithm are successfully transitioned into a higher-fidelity ephemeris

model with solar and lunar gravitational perturbations. Sliding geometry transfers are transitioned into the higher-fidelity ephemeris model from either a converged solution in the CRTBP-LT model, or, from a set of periodic orbits generated as the initial guess by the sliding algorithm. The roughness parameter maps aid in generalizing this transition, by offering a range of possible epochs that reduce the sensitivity of the problem, and guarantees a smooth performance of the multiple shooting corrections process. The weighting parameters in the objective function in the adaptive sliding algorithm are easily modified to accommodate either mass-optimal or time-optimal solutions. Regardless of the prioritization for this minimization function, the algorithm delivers a locally optimal solution with the minimum number of intermediate orbits from departure to destination.

ACKNOWLEDGMENTS

The authors would like to thank the members of the Multibody Dynamics Research Group at Purdue University, as well as the Visualization lab for use of computing resources. Portions of this work were supported by the Purdue University Minority Engineering Program. The authors also appreciate partial support from NASA Grant 80NSSC20K1117.

REFERENCES

[1] Hambleton, K. "Deep Space Gateway to Open Opportunities for Distant Destinations." NASA, (March 28, 2017) *https://www. nasa. gov/feature/deep-space-gateway-to-open-opportunities-for-distant-destinations*. 24 August 2018

[2] Folta, D.C., Bosanac, N., Cox, A. and Howell, K.C. "The Lunar IceCube Mission Design: Construction of Feasible Transfer Trajectories With a Constrained Departure." *AAS/AIAA Space Flight Mechanics Meeting*, February 2016, AAS 16-285.

[3] McGuire, M.L., Burke, L.M., McCarty, S.L., Hack, K.J., Whitley, R.J., Davis, D.C. and Ocampo, C. "Low Thrust Cis-Lunar Transfers Using a 40 KW-Class Solar Electric Propulsion Spacecraft." *AAS/AIAA Space Flight Mechanics Meeting*, February 2017, AAS 17-583.

[4] Pritchett, R., Zimovan, E. and Howell, K.C. "Impulsive and Low-Thrust Transfer Design between Stable and Nearly Stable Periodic Orbits in the Restricted Problem." *18th AIAA SciTech Forum*, Kissimmee, Florida, January 2018.

[5] Ashwati Das-Stuart. "Artificial Intelligence Aided Rapid Trajectory Design in Complex Dynamical Environments." Ph.D. Dissertation, Purdue University, West Lafayette, Indiana, 2019.

[6] Lantoine, G. "Efficient NRHO to DRO Transfers in Cislunar Space." In *AAS/AIAA Astrodynamics Specialist Conference*, August 2017, pp. 1-18.

[7] Williams, J., Lee, D.E., Whitley, R.J., Bokelmann, K.A., Davis, D.C. and Berry, C.F. "Targeting Cislunar Near Rectilinear Halo Orbits for Human Space Exploration." *AAS/AIAA Spaceflight Mechanics Meeting*, February, 2017.

[8] Howell, K.C. and Breakwell, J.V. "Almost Rectilinear Halo Orbits." *Celestial mechanics*, 32(1), pp.29-52.

[9] Szebehely, V. "Theory of Orbits: The Restricted Problem of Three Bodies." Yale Univ New Haven, CT, 1967.

[10] Newton, I. "The Principia: Mathematical Principles of Natural Philosophy." University of California Press, California, USA, 1999.

[11] Barrow-Green, J. "Poincaré and the Three Body Problem." No. 11, History of Mathematics, American Mathematical Society, Providence, Rhode Island, 1997.

[12] Cox, A. D., Howell, K. C., and Folta, D. C., "Trajectory Design Leveraging Low-Thrust, Multi-Body Equilibria and their Manifolds." *Journal of the Astronautical Sciences*, 14 April, 2020.

[13] Haapala, A. and Howell, K.C. "Representations of Higher-Dimensional Poincare Maps with Application to Spacecraft Trajectory Design." *Acta Astronautica*, 96, 2014, pp. 23-41.

[14] Amanda F. Haapala. "Trajectory Design Using Periapse Maps and Invariant Manifolds." M.S. Thesis, Purdue University, West Lafayette, Indiana, 2010.

[15] Grebow, D.J., Ozimek, M.T. and Howell, K.C. "Design of Optimal Low-Thrust Lunar Pole-Sitter Missions." *The Journal of the Astronautical Sciences*, 58(1), 2011, pp.55-79.

[16] E.S. Gadelmawla, M.M. Koura, T.M.A. Maksoud, I.M. Elewa, H.H. Soliman. “Roughness Parameters.” *Journal of Materials Processing Technology*, 123, 2002, pp. 133-145.

[17] Senent, J., Ocampo, C. and Capella, A. “Low-Thrust Variable-Specific-Impulse Transfers and Guidance to Unstable Periodic Orbits.” *Journal of Guidance, Control, and Dynamics*, 28(2), 2005, pp.280-290.

[18] Stuart, J., Ozimek, M. and Howell, K. “Optimal, Low-Thrust, Path-Constrained Transfers Between Libration Point Orbits Using Invariant Manifolds.” In *AIAA/AAS Astrodynamics Specialist Conference*, 2010, p. 7831.